SPECTRAL-ANGULAR CHARACTERISTICS OF THE LCLS IN THE NEAR AND FAR FIELDS*

R. Tatchyn[#], SSRL, Stanford, CA 94305, U.S.A.

Abstract

The unusually long insertion devices being prepared for Angstrom-wavelength Free Electron Lasers (FELs) will generate spectral-angular distributions in the proposed experimental areas substantially different from those conventionally calculated for the far field. In this paper we report on computational simulations of near vs. far field distributions for the SLAC linac Coherent Light Source (LCLS) undulator, an insertion device approximately 140 meters long. The properties of the coherent radiation as a limiting case of the near-field emission, for the special condition of a microbunched beam radiating along the undulator axis, are reviewed.

INTRODUCTION

A number of the pending or proposed generations of synchrotron radiation (SR) research facilities centered on linac driven Ångstrom-wavelength Free Electron Lasers (FELs) operating in the Self-Amplified Spontaneous Emission (SASE) [1] regime will feature undulators of unprecedented length. For example, the SLAC Linac Coherent Light Source (LCLS) is being developed around a 140 meter long device [2], while the DESY-based TESLA FEL facility has proposed a multi-undulator switchyard with device lengths ranging from ~100 meters to more than 300 meters [3,4]. In contrast to storage ring based undulator beam lines, on which the distance from the undulator to the experiment is typically approximately 10 times (or more) greater than the insertion device length, the corresponding factor for both the LCLS and some of the TESLA beam lines will be substantially smaller. In the case of the LCLS, for example, the nearest beam diagnostics detectors could be located as a close as ~10–40 meters from the undulator exit, while the farthest possible experimental location will still be less than 6 insertion device lengths away from the undulator exit. For such significantly reduced distance/length ratios it is no longer possible to represent, in general, the spontaneous radiation emitted by an electron passing through the undulator by the conventional far-field formalisms widely employed at present-day storage ring Synchrotron Radiation (SR) facilities [5] and a revised formalism accounting for the detailed near-field characteristics of the emitted radiation must be developed [6].

In this paper the structure of one such formalism will be outlined and a set of illustrative spontaneous radiation calculations contrasting the far-field vs. near-field spectral-angular distributions of the LCLS will be presented. The significance of the results for simulations of the full LCLS FEL spectrum will be discussed and a systematic algorithm for accomplishing this will be outlined.

NEAR-FIELD VS. FAR-FIELD REGIMES: GEOMETRICAL DEPENDENCE

A conventional representation of an observation plane centered at normal incidence on an undulator axis is shown in Fig. 1. P denotes the on-axis observation point, P' a general off-axis observation point, and d the distance from the axis to P'. Our conventional assumption will be that an electron enters the undulator at A, passes through N periods of length λ_u, emerges at B, and that it is accelerated, i. e., emits radiation, only between A and B.
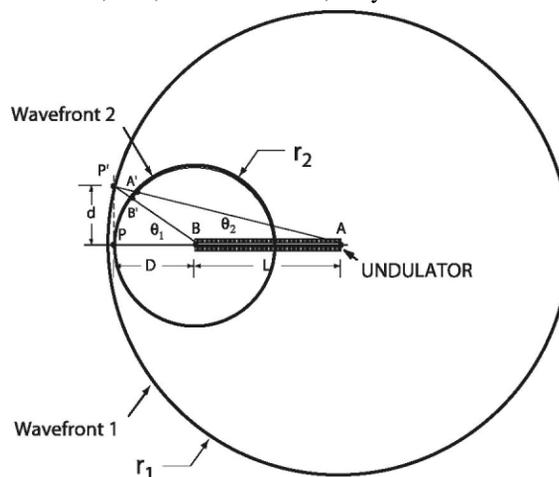
Figure 1: Near-field effects of an N-period undulator. ABP' is rotated about AB to lie in the plane of the paper.

To illustrate the different types of near-field effects and the parameters that govern them, the initial and final signal waves emitted by the electron as it passes points A and B along the undulator axis are represented by spherical wavefronts. We note that, apart from the geometry, the average velocity of the electron through the undulator will evidently also determine the time interval between the wavefronts observed at either P or P' and, of course, the detailed (instantaneous) spectral-angular distribution of the observed radiation.

Referring to the above construction, the following geometrical effects on the radiation observed at off-axis observation point P' can be identified:

a. a wavelength chirp as the wavefronts from the N successive periods of the undulator arrive at P', the first one along $P'A'$ and the final one along $P'B'$. This chirp disappears at P.

b. a corresponding angular chirp of the incoming Poynting vector at P', which also disappears at P.

c. for a fixed-area infinitesimal aperture at *P'*, the electric field amplitude of the normal component of the observed radiation-field wavefront 1 is inversely proportional to r_1 and directly proportional to a factor of between 1 and $\cos\theta_2$. Similarly, the normal component of wavefront 2 is inversely proportional to r_2 and directly proportional to a factor of between 1 and $\cos\theta_1$. Thus, under the condition $\cos\theta_2 \sim \cos\theta_1 \sim 1$, the net result is a field amplitude chirp at *P'* that is inversely proportional to the monotonically decreasing radii of the *N* successive wavefronts impinging on the observation aperture. This chirp (of geometric origin) is present in addition to the spectral-angular amplitude variation associated with the strongly anisotropic spectral-angular distribution of a relativistic electron's emitted radiation. As opposed to effects a. and b., this (radius-dependent) amplitude chirp is always observed at *P*.

With regard to the construction parameters in Fig. 1, we can straightforwardly establish conditions under which these effects constitute only small departures from a far-field spectral-angular distribution. For specificity, we consider the undulator's fundamental line, for which the far-field bandwidth and angular full width at half-maximum (FWHM) are give by, respectively, $1/N$, and $\sqrt{(2+K^2)/N}/\gamma$, where $K\,(\cong 0.934\,B[T]\lambda_u[cm])$ is the undulator parameter; *B* is the undulator field amplitude; and γ is the Lorentz factor of the bunch [7]. Thus, for the amplitudes of wavefronts 1 and 2 to attain a relative difference of η_1 or less at *P*, we find

$$\left(\frac{1}{D}-\frac{1}{L+D}\right)(L+D)=\frac{L}{D}\le\eta_1 \qquad . \qquad (I)$$

For an angular chirp AT *P'*, relative to the (far-field) fundamental, of η_2 or less, we derive

$$(\theta_1-\theta_2)\,\gamma\sqrt{\frac{2N}{1+K^2/2}}\cong\frac{dL}{D(D+L)}\left(\gamma^*\sqrt{2N}\right)\le\eta_2 \quad , \quad (II)$$

Where $\gamma^* = \gamma\sqrt{1+K^2/2}$, and for a corresponding wavelength chirp at *P'*, relative to the (far-field) bandwidth $1/N$, of η_3 or less,

$$\frac{(\gamma^* d)^2 L(L+2D)}{D^2((D+L)^2+(\gamma^* d)^2)}\,N\le\eta_3 \qquad . \qquad (III)$$

Considering the LCLS, numerical values for each of these parameters are readily computed and demonstrate that at all the experimental or diagnostics locations within the boundaries of SLAC near-field effects will significantly influence or dominate both the spontaneous and coherent spectral-angular distributions [8]. These results, which also illustrate the decreasing influence of near-field effects vs. increasing distance from the undulator exit, tend to corroborate the commonly accepted practice of disregarding near-field effects for dimensional ratios *D/L*>10 *and* observation points not too far off the axis, conditions pertaining to most present-day storage ring undulator beam lines (however, in this regard see [9]), and this implies an analogous scaling of *D* into the several-kilometer regime in order for the x-ray SASE FELs of the present era to operate in the sane limit.

NEAR-FIELD VS. FAR-FIELD REGIMES: ANALYTICAL FORMULATION

To construct the analytical formalism for calculating the spectral-angular flux distribution observed at *P'* we refer to the general vector parameters shown in Fig. 2. For our purposes we will locate the fixed point *O* midway between *A* and *B* on the undulator axis (see Fig. 1) and assume *P'* to be located in the observation plane, which lies normal to the undulator axis. Given these assumptions it is evident that the average direction of the trajectory vector *r* will be parallel to the undulator axis and that the deviation from parallelism for practical undulator and electron beam parameters will be very small.
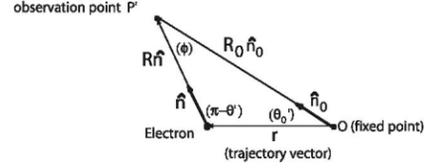
Figure 2: Vector construction and analytical parameters used for calculating the radiation from an accelerated electron at *P'*.

Given the fact that most practical experiments accept synchrotron radiation through an aperture of fixed area and position and that both the direction and location of the electron with respect to such an aperture can vary considerably in the near field, the concept of a fixed solid angle defined by the aperture with respect to the electron becomes indefinite over the course of its acceleration. Due to this, the near-field formalism most appropriate for evaluating the flux impinging on the aperture should directly evaluate the Poynting vector of the electron's radiation at *P'*. This means that the temporal signal of interest will be the retarded electric radiation field (since the Poynting vector can be calculated directly from it) and that the corresponding spectral signal observed at *P'* will be just the Fourier transform of this retarded electric field. Formulas for the spectral-angular distribution associated with the retarded radiation field of an electron have been discussed by a number of prior authors, e.g., Jackson [10], and we present a related formulation applicable to the parameter range we are investigating here:

$$\frac{dI_1(f)}{d\Sigma(df/f)}=\frac{q^2 f}{4\pi^2 c}\left|\int_{-\infty}^{\infty}\frac{\hat{n}\times\left[(\hat{n}-\boldsymbol{\beta})\times\dot{\boldsymbol{\beta}}\right]}{(1-\hat{n}\cdot\boldsymbol{\beta})^2 R}e^{2\pi i f(t'+[R(t')/c])}dt'\right|^2 . \quad (1)$$

Here the units of the spectral-angular density are Joules per second per unit area per unit bandwidth, $d\Sigma$ denotes a unit increment of area lying in the observation plane at *P'*, $\boldsymbol{\beta}=\dot{n}/c$, $\dot{\boldsymbol{\beta}}=\ddot{n}/c$, *t'* is the retarded time at which all the parameters in the integrand of (1) are evaluated, and the physical constants are in MKS units. For simplicity, an inclination factor accounting for the angle of incidence and polarization of the radiation falling on Σ has been omitted, as for the majority of practical x-ray FEL configurations the deviations of this angle from normal incidence will be very small. As *R* increases to the point that it becomes approximately constant over the length of

the undulator, it can be shown [8] that expression (1) begins to approximate to the conventional spectral-angular distribution widely utilized for calculations at most present-day storage ring installations [11,12].

CALCULATIONS OF LCLS SPONTANEOUS RADIATION IN THE NEAR-FIELD VS. FAR-FIELD REGIMES

Although it is possible to integrate (1) directly for an arbitrary trajectory vector **r,** a substantial algorithmic simplification can be achieved by taking advantage of the natural periodicity of the undulator field. For example, for an *N*-period device (with *N* large enough to allow omission of a detailed description of the end-field regions without affecting the required accuracy or validity of the computed spectra), (1) can be rewritten as

$$\frac{dI_1(f)}{d\Sigma(df/f)} = \frac{q^2 f}{4\pi^2 c}\left|\sum_{j=1}^{N}\left\{\int_{-L/2+(j-1)\lambda_u}^{-L/2+j\lambda_u}\frac{\hat{n}\times\left[(\hat{n}-\boldsymbol{\beta})\times\dot{\boldsymbol{\beta}}\right]}{(1-\hat{n}\cdot\boldsymbol{\beta})^2 R}e^{2\pi i f(t'+[R(t')/c])}dt'\right\}\right|^2 . \quad (2)$$

In the case of the LCLS, it is then readily apparent that even at the closest distance of a detector to the undulator exit (viz., ~10 m) the condition $D \gg \lambda_u$ will apply, i.e., the radiation arriving at Σ from each individual undulator period can be accurately described by its far-field form. This leads to the following expression, whose integral is readily computable with well-known and relatively straightforward numerical algorithms [12].

$$\frac{dI_1(f)}{d\Sigma(df/f)} \cong \frac{q^2 f}{4\pi^2 c} \quad\quad\quad\quad . \quad (3)$$

$$\times\left|\sum_{j=1}^{N}\left\{\frac{e^{2\pi i f R_{0j}/c}}{R_{0j}}\int_{-L/2+(j-1)\lambda_u}^{-L/2+j\lambda_u}\frac{\hat{n}\times\left[(\hat{n}-\boldsymbol{\beta})\times\dot{\boldsymbol{\beta}}\right]}{(1-\hat{n}\cdot\boldsymbol{\beta})^2 R}e^{2\pi i f(t-\bar{n}_{0j}\cdot\boldsymbol{r}(t)/c)}dt\right\}\right|^2$$

For the LCLS, whose current design features a 3 cm period and thirty-three 4-m-long field segments interleaved with thirty-two 30 cm long drift spaces [2], the form of (9) is optimal, as the drifts are approximately $10\lambda_u$ long and the algorithm simply sets the acceleration to 0 as the particle moves through each drift section. In practice, rather than calculating each period, the undulator, as well as the drifts, can each be subdivided into longer segments L_u' and L_D', with $D \gg L_u'$, L_D', to further economize the computation.

In Figs. 3–5 both the far-field and near-field angular flux distributions of the LCLS fundamental corresponding to (3) are plotted for the nominal operating current of the LCLS (3400 A) at three different distances (9 m, 40 m, and 380 m) from the undulator exit for a limiting operating energy of 14.34 GeV. No FEL bunching is assumed and electron beam emittance effects are not included. We note that the abscissas display distance away from the undulator axis, along the horizontal axis of observation (i.e., for *y*=0) in the observation plane. In this regard, it should be emphasized that the ordinate units have a well-defined meaning only for the far-field curve displayed in each graph; a more complex interpretation is required for the near-field curves. With regard to the curve shapes, we
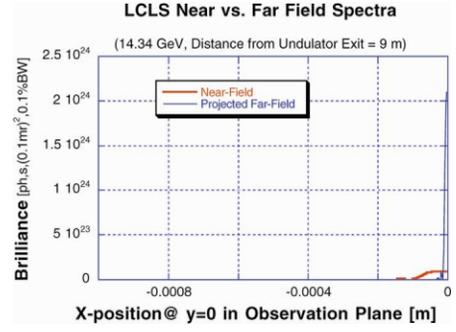
Figure 3: Far-field vs. near-field flux distributions of the LCLS fundamental. *E*=14.34 GeV, I_u=3400 A.
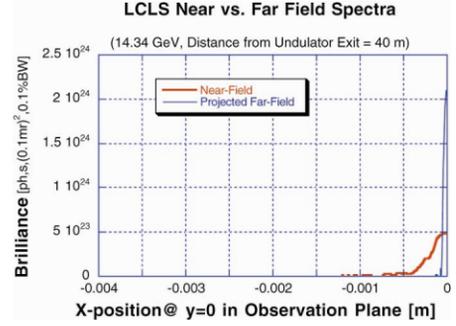
Figure 4: Far-field vs. near-field flux distributions of the LCLS fundamental. *E*=14.34 GeV, I_u=3400 A
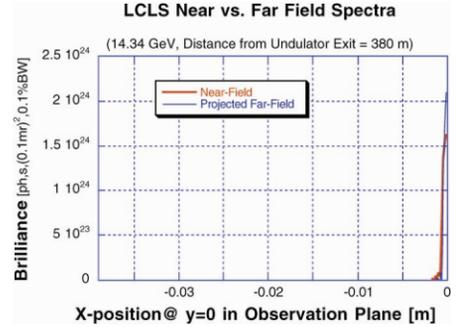
Figure 5: Far-field vs. near-field flux distributions of the LCLS fundamental. *E*=14.34 GeV, I_u=3400 A

first note that the far-field-curves at each energy are identical in angular profile and amplitude regardless of distance away from the undulator exit, as expected. The deviations of the near-field curves' shapes from those of the far field are seen to be primarily governed – for the particular range of parameters chosen – by criterion I, viz., the effect of amplitude variation of the radiation arriving at the observation plane, i.e., due to the strongly varying relative distances of successive segments of the undulator from the detector. This causes the spectral-angular distribution to be dominated by the undulator sections closest to the observation point, and since their total number of periods is necessarily < *N*, the corresponding spectrum is both attenuated and broadened.

LCLS COHERENT VS. SPONTANEOUS RADIATION SPECTRA

In view of the fact that a SASE FEL accepts no external (exogenous) radiation, it can be shown that the amplitude of the total radiation field must be strictly equal to the linear superposition of the amplitudes associated with the individual bunch electrons. If we interpret each amplitude to be a functional of its associated electron's trajectory vector $\boldsymbol{r}_n$ (where n is used to index the N_e bunch electrons), we obtain

$$\frac{dI_1(f)}{d\Sigma(df/f)} = \frac{q^2 f}{4\pi^2 c}$$

$$\times \left| \sum_{n=1}^{N_e} \left\{ \int_{-\infty}^{\infty} \frac{\hat{\boldsymbol{n}}_n \times \left[(\hat{\boldsymbol{n}}_n - \boldsymbol{\beta}_n) \times \dot{\boldsymbol{\beta}}_n \right]}{(1 - \hat{\boldsymbol{n}}_n \cdot \boldsymbol{\beta}_n)^2 R_n} e^{2\pi i f (t' + [R_n(t')/c])} dt' \right\} \right|^2 \quad . \ (4)$$

To derive $\boldsymbol{r}_n$ for any particular FEL electron, the conventional analytical procedure is to solve the non-linear equations governing the dynamics of the FEL gain process (q.v., e.g., [1]). Common to many such analyses is the representation of the bunching process as an instability in the electron beam current that develops in response to the interaction of random density fluctuations in the electron bunch with the undulator field. In this regard, the corresponding analyses of the bunching dynamics typically focus on fields averaged over large sub-populations of the bunch's electrons, i.e., the derived parameters governing the bunching process are themselves inherently statistical in nature. This stricture applies equally to most of the FEL computer simulation codes in present use, where it still remains infeasible to iterate N_e^2 equations (for $N_e \sim 10^7 - 10^9$) through a several-thousand period undulator, in consequence of which the inherently statistical construct of a "macroparticle" is employed to simulate the approximate average effects of bunching on a particle trajectory. In view, then, of the statistical nature of presently available SASE FEL bunching parameters, it appears reasonable to consider them, along with (4), as a basis for comparably valid, yet substantially more economical, Monte Carlo simulations of the spectral-angular output of a SASE FEL.

As has been shown by a number of prior authors (e.g., [13]), the $\boldsymbol{r}_n$ of a SASE FEL electron in fact differs very little from its unmodulated trajectory (which faithfully tracks the undulator's periodic field profile). The basic FEL departure from this ideal periodic profile can be represented as a longitudinal position-energy modulation of the trajectory's sinusoidal components. If the undulator field is sinusoidal, the analytical description of FEL bunching becomes closely analogous to that of a Phase Modulated (PM) wave [14]. Thus, an electron trajectory in an FEL can be approximated by a phase-space modulated periodic trajectory depending on essentially three constituents: 1) the distribution of longitudinal positions and energies in the undulator at which the phase space modulation starts; 2) the set of phase space distributions toward which the particle's longitudinal position and energy tend; and 3) the distribution of time-dependent amplitudes and functional profiles of the phase space motion between the starting positions and energies and those at the undulator exit. Given that these three sets can be represented by a sufficiently small set of statistical parameters (derivable, in principle, from the equations governing SASE FEL dynamics), a representative spectral-angular SASE FEL distribution from a SASE bunch can then be computed in a time ~proportional to N_c, the number of electrons in a cooperation length [13]. The incorporation of such parameters into $\boldsymbol{r}_n$ and numerical studies of how they combine to define the coherent line output of the LCLS will be pursued in future studies.

REFERENCES

[1] K.-J. Kim, "Three Dimensional Analysis of Coherent Amplification and Self-Amplified Spontaneous Emission in Free-Electron Lasers," PRL 57(13), 1871 (1986).

[2] J. Arthur et al., "Linac coherent light source (LCLS) conceptual design report," SLAC-R-593; UC-414; 2002; http://www-ssrl.slac.stanford.edu/lcls/cdr/

[3] K. Floettmann (for the TESLA Collaboration), "The TESLA Linear Collider And X-Ray FEL," Proceedings of LINAC 2002, Gyeongju, Korea, August 19-23, 2002.

[4] TESLA Technical Design Report, DESY Report No. 2001-11, DESY, Hamburg, Germany, 2002.

[5] S. Krinsky, M.L. Perlman, R.E. Watson, "Characteristics of synchrotron radiation and of its sources," in Handbook on synchrotron radiation, E.E. Koch, ed., North-Holland, Amsterdam, Neth., 1983, pp. 65-171.

[6] R. Tatchyn et al., "X-ray Optics Design Studies for the 1.5-15 Å Linac Coherent Light Source (LCLS) at the Stanford Linear Accelerator Center (SLAC)," SPIE Proceedings 3154, 1997, pp. 174-222.

[7] K.-J. Kim, "Characteristics of synchrotron radiation," in X-Ray Data Booklet, A. Thomson et al, eds. Center for X-Ray Optics, LBNL/PUB-490 Rev, 2001, pp. 2-6–2-7.

[8] R. Tatchyn, "An analysis of near-field vs. far-field radiation characteristics of the Linac Coherent Light Source," LCLS-TN-05-2, SLAC-TN-05-046, http://www-ssrl.slac.stanford.edu/lcls/technotes

[9] R.P. Walker, "Near Field Effects in Off-axis Undulator Radiation," NIM, A267, 1987, p. 537.

[10] J. D. Jackson, Classical Electrodynamics, John Wiley & Sons, New York, 1975, pp. 662-671.

[11] R. Coisson and R. Tatchyn, "Introduction to Optical Properties of Insertion Devices Excited by Synchrotron Sources," in Tutorial T1, International Conference on Insertion Devices for Synchrotron Sources, SSRL, Stanford University, October 27, 1985, SPIE Proceedings No. 582, 1986.

[12] R. Tatchyn. A.D. Cox, S. Qadri, "Undulator Spectra: Computer Simulations and Modeling," SPIE Proceedings No. 582, 1986, p.47.

[13] W.B. Colson, "Classical free electron laser theory," in Free Electron Laser Handbook, W.B. Colson, C. Pellegrini, A. Renieri, eds., North-Holland Physics, Elsevier, The Netherlands, 1990, Ch. 5, pp. 115-194.

[14] H. Taub, D.L. Schilling, Principles of Communication Engineering, McGraw-Hill Book Company, New York, 1971, pp. 114-131.